Winter 2022

The Influence of Permafrost Soil Structure on Microbial Community Diversity and Abundance

nathan D. blais
University of New Hampshire, Durham

The Influence of Permafrost Soil Structure on Microbial Community Diversity and Abundance

By

Nathan Blais

BS Environmental Science, University of New Hampshire, 2019

THESIS

Submitted to the University of New Hampshire

in Partial Fulfillment of

the Requirements for the Degree of

Master of Science

in

Natural Resources and the Environment

December 2022

This thesis was examined and approved in partial fulfillment of the requirements for the degree of Master's in Natural Resources and the Environment by:

Thesis Director, Jessica Ernakovich, Ph.D.
Professor of Natural Resources and the Environment

Robyn Barbato, Ph.D.
Research Scientist: Cold Research and Engineering Lab

Alexandra Contosta, Ph.D.
Research Assistant Professor: Earth Systems Research Center

On September 1st, 2022

Approval signatures are on file with the University of New Hampshire Graduate School.

ACKNOWLEDGEMENTS

I would like to thank all of my friends and family for their continued support during my academic career.

I also thank everyone who has supported my work including Dr. Buck Castillo, Dr. Hannah Holland-Moritz, Joy O'Brien, Julie Bobyock, Lukas Bernhardt, Dr. Erin Rooney, Lauren Farnsworth, Dr. Zoe Courville, Dr. Tom Douglas, Dr. Vanessa Bailey, Dr. Taylor Sullivan and my past and present Ernakovich lab members. The contributions of these folks have been critical to the completion of my degree.

A special thanks goes to Dr. Alix Contosta and Dr. Robyn Barbato whose contributions as committee members and mentors through my undergraduate and graduate experience has shape who and where I am today as a scientist.

Most importantly, I thank my advisor Dr. Jessica Ernakovich. Jessica has been instrumental to my development and success in my career. It has been and continues to be an incredible opportunity to work with such a caring and inspiring advisor.

Lastly, I would like to thank my funding sources including the Department of Natural Resources here at the University of New Hampshire, The NASA New Hampshire Space Grant Consortium, The Applied Research Funding for Extreme Cold Weather through the ASA (ALT) and AFC, and UNH Collaborative Research Excellence Initiative.

Table of Contents

ABSTRACT

Soil structure plays a critical role in shaping soil microbial communities, who directly influence biogeochemical cycling[1–4]. Although well-studied in temperate systems, the importance of physical structure on soil microbial community diversity, function, and overall activity in permafrost soils is largely unknown. I hypothesized that (1) decreases in pore connectivity would increase microbial diversity based on an expected inverse relationship between diversity and connectivity; (2) soil with an increased abundance of larger pores (> 75 μm), which are uninhabitable because they are too large to sustain liquid water, will exhibit lower bacterial and archaeal abundance and (3) the surface area of ice inclusions, which represents potentially habitable space in the form of brine channels, will be positively correlated with the abundance of active microbes. To test these hypotheses, I analyzed eight permafrost cores from three distinct sites in Alaska. Fine scale heterogeneity in soil physical and biological characteristics was captured from triplicate subsamples per core. To quantify soil ice inclusions and pore architecture, I scanned permafrost at -10 ºC using X-ray Computed Tomography to maintain its structure. Following scanning, both DNA and RNA were extracted from the permafrost and analyzed via amplicon sequencing and quantitative PCR of the 16S region. I analyzed the total and active microbial community diversity, and abundance. I found that at a scanning resolution of 20 μm only macro-scale features (>75 μm) could be quantified. Despite the limitation to the resolution, permafrost soil appears to share characteristics with temperate soils like the dominant pore size class (75-100 μm) and the positive relationship between total porosity and pore connectivity. I also found a negative relationship between macroporosity and microbial diversity, indicating that dispersal limitation in permafrost and past soil conditions may contribute to the spatial structure of microbial community diversity currently seen in permafrost.

Additionally, soil structure did not influence the abundance of the active microbial community, indicating. I require finer scale structural and microbial data to disentangle any existing relationships. Gaining these insights could help us understand how soil physical structure acts to influence community structure in this extreme environment.

1. INTRODUCTION

Soil physical structure is increasingly recognized for its role in shaping soil microbial communities, which mediate biogeochemical cycling[1–4]. One of the most important aspects of soil structure are pore networks[5–7]. Pore structure can impact carbon and nutrient cycling by physically protecting organic matter and by controlling the distribution and movement of water, air, nutrients, and microbes through the soil matrix[2,3]. Despite extensive research in unfrozen systems, it is unclear if soil structure has an impact on microbial activity, diversity, and soil processes in permafrost, or perennially frozen soil systems. In permafrost there are significant challenges to the metabolic activity of microbes, such as sub-zero temperatures[8], high ice content [9], low water availability[10], and energetically unfavorable resources[11]. Additionally, as in non-permafrost or unfrozen soils, the state and distribution of water is essential to shaping microbial communities in permafrost[10]. Thus, permafrost structure—including pore and ice structure—is likely to influence microbial community dynamics in addition to known factors like organic matter chemistry, pH, and temperature.

One of the most important characteristics of soil pore structure which influences microbial activity are pore size classes. In temperate soils, pore size classes tend to exhibit predictable patterns of carbon mineralization, a proxy for activity[1,12–15]. The smallest pore and throat (pore openings) size classes, generally <10-30 μm, protect soil organic matter and limit decomposition because they limit physical accessibility by microbes and are often water filled, further limiting aerobic decomposition[1,13–15]. Larger pores and throats, roughly 30-150 μm, enhance organic matter decomposition as these pores allow for increased hydrologically connectivity and aeration[1,14,15]. Lastly, macro pores (>150 μm) limit decomposition as they are mostly air filled [12,15] with the potential to indirectly increase decomposition through increased

aeration of smaller surrounding pores[1]. In addition to soil pore size classes, pore connectivity, or how often pores intersect with other pores, is a critical component of soil pore structure. Soil pore connectivity influences the transport of air and water, and thus resources and microbes through the soil[16,17]. Specifically, pore connectivity has been proposed as a core driver of microbial diversity in temperate soils[18,19]. Bacterial diversity in soils has been found to increase with decreasing pore connectivity[18–20]. The proposed mechanism for this relationship is that low connectivity restricts microbial and substrate movement in pore water and reduces the selective force of competition between organisms[18,19,21]. Both pore connectivity and pore size classes have yet to be quantified in permafrost or studied in relation to microbial community diversity but could have a similar influence on microbial communities to that of temperate soils.

In frozen soil, the total water potential determines the freezing point of water, controlling the amount of water that remains unfrozen[22] and consequently the habitable space available for metabolically active microbes in permafrost[10,23]. One key component of the total water potential is the osmotic potential which is largely determined by dissolved solute concentration. Solutes become more concentrated as water freezes, which decrease the freezing point of water[24] and in mineral dominated soils this is the main mechanism determining unfrozen water content[25]. In soils with more organic matter the matric potential (the attraction of water to soil)[26] governed largely by pore size distributions, plays an important role in regulating the amount of unfrozen water in the soil. Using matric potentials in Swedish O-horizon spodozol soils, Harryson et al. (2009) determined the theoretical maximum pore size that can hold liquid water at -4°C to be around 0.2 μm. However, considering the osmotic potential, the actual size of pores able to sustain liquid water may be larger[24]. In these organic soils the largest pore sizes capable of supporting liquid water (~ 0.2 μm) were shown to correspond to higher rates of microbial

respiration (indicative of microbial activity) compared to smaller pore size classes (~ 0.1 μm)[23]. Further, pore size distributions may shape the role of pore connectivity in permafrost soils. The connectivity of small water-holding pores may influence the diversity and the availability of resources like larger water filled pores in unfrozen soil[18–20], while connectivity among larger air-filled pores in permafrost may impede this underlying connectivity because they are void of unfrozen water or hydrologically disconnected. Thus, like unfrozen soil, in permafrost or seasonally frozen soil, pore size distributions and pore connectivity likely influence the movement of microbes and resources through their influence on water, and likely influences microbial community abundance and diversity.

While both unfrozen and frozen soil share many physical characteristics (e.g., pores of varying size classes), a major structural distinction between the two is the presence of ice. Ice can form in the smallest of pores to massive wedges meters in size. One key feature of many mineral permafrost soils—as opposed to unfrozen or seasonally frozen soils—is segregated ice, where there is a clear delineation between ice and soil, and this often appears in layers called lenticular structures[27]. These soils are laced with a complex matrix of solid ice. When lenticularly structured permafrost is formed, the soil layers dry and liquid water retreats to the area just around the layers of ice[9]. These ice inclusion "neighborhoods" may represent potentially habitable space for active microbes. Heterogeneity in the surface area of this ice could influence the spatial distribution of active microbes and overall microbial activity in lenticularly affected permafrost soils.

Historically, the characterization of fine scale permafrost structure has been limited to the unaided eye and 2-D microscopy[27]. While these techniques can effectively identify and classify soils based on their attributes like ice structure and soil texture, they fall short in their inability to

quantify the three-dimensional nature of these features. High Resolution X-ray Computed Tomography (micro-CT scanning) is an effective way to characterize and quantify 3-D soil structures. Micro-CT scanning is a tool often associated with the health industry but also has a wide range of environmental uses. In permafrost research the utilization of micro-CT scanning has been limited primarily to the geosciences for quantifying ice, gas, and sediment composition on a macro scale (>mm)[28–30]. In temperate soils, micro-CT scanning has been utilized to explore soil porosity, pore throat size, and connectivity[3,15,31,32]. To our knowledge studies have yet to explore and quantify intact permafrost soil structure at the micro scale to investigate its influence on the soil microbiome. A deeper knowledge of the factors structuring microbial communities in frozen permafrost may inform our understanding of how these communities are affected by disturbance like warming thaw events.

To better understand the micro-structures within permafrost soils and their influence on permafrost soil microbiomes I used micro-CT scanning to scan eight permafrost cores from three distinct sites in the interior of Alaska using micro-CT scanning and characterized the microbial community using DNA and RNA amplicon sequencing and quantitative PCR of the 16S rRNA gene region. I sought to answer two principal questions: 1) What is the fine scale (<100 µm) heterogeneity in permafrost soil structure within and between sites? and 2) What is the relationship between soil structure and microbial diversity and abundance? I hypothesized that (1) there would be an inverse relationship between pore connectivity and microbial diversity due to connectivity increasing the selective force of competition subsequently reducing diversity; (2) soil with an increased abundance of larger pores, which are assumed to be uninhabitable because they are too large to sustain liquid water, would have lower bacterial and archaeal abundance and (3) the surface area of ice inclusions, which represent potentially habitable space, would be

positively correlated with the abundance of active microbes. Our results shed light onto the impactful role of pore space in shaping microbial community diversity in permafrost as well as the challenges and limitations of scanning permafrost soils.

2. METHODS

2.1 Site Information, Sample Acquisition, and Preparation:

We analyzed eight permafrost cores from three locations: (1) Above the Cold Regions Research and Engineering Lab (CRREL) tunnel in Fox, Alaska, which is a mineral dominated permafrost; (2) Farmers Loop, Alaska, a highly organic permafrost; and (3) Utqiagvik, Alaska, a mineral permafrost also rich in organic matter (Fig 1). Cores were extracted from the permafrost

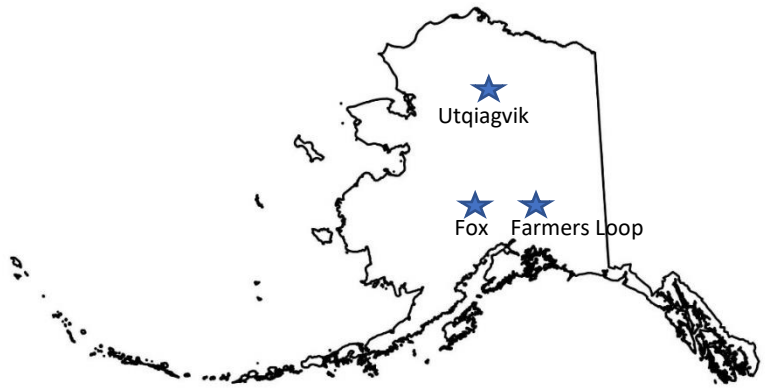

Fig. 1) Blue arrows indicate the locations of the three study sites in Alaska, USA. Fox, Farmers Loop, and Utqiagvik.

using a SIPRE corer (Jon's Machine Shop, Fairbanks, AK) and were approximately a meter in length (25 cm core sections) and 10 cm in diameter. Cores were shipped to the University of New Hampshire in coolers with dry ice to maintain subzero temperatures and then stored at -20 ºC.

Prior to analysis, ~ 0.5 cm of soil was scraped with a sharp paint scraper aseptically from the sides of all cores in a walk-in freezer (~ -7°C) to remove potential microbial contamination. Next, with a carbine tooth saw bit attached to an electric drill I extracted three permafrost pucks ~1 cm in height and 2.5 cm in diameter from each core at approximately 5 cm below the seasonally thawed active layer. Soil pucks were immediately placed in sterile plastic containers

and stored at -20 ºC until the time in which they would be scanned. Personnel working with samples all had Tyvek suits (Wilmington, DE, United States) on and before processing and between samples all tools were sterilized with 70% ethanol or autoclaving.

2.2 High Resolution Micro X-ray Computed Tomography:

Permafrost samples (individually drilled pucks) were scanned at the Cold Regions Research and Engineering Lab in Hanover, New Hampshire using a Bruker Skyscan 1173 micro-CT (Bruker, Billerica, MA, USA). The scanner was in a walk-in cold room set to approximately -10°C to prevent sample thawing during scanning. Scanner settings were 100 kV source voltage, 62 µA source current, 250 ms exposure, and 20 µm resolution. An aluminum filter was used during all scans. Each sample was scanned for ~20 minutes and yielded ~ 1500 continuous image slices.

2.3 Image Processing and Segmentation:

Post-scan reconstruction was performed in the Bruker Micro-CT Software: CT-Analyser (Blue Scientific, Cambridge, England). In CT-Analyser, image stacks were automatically corrected for ring and beam hardening artifacts[33]. Corrected CT-Analyser image stacks were then converted to PNG files and imported to Dragonfly image processing and analysis software (Object Research Systems, Montreal, Canada). To prepare images for segmentation, I applied a tv-chambolle denoising filter to eliminate speckle noise[34].

Image segmentation of regions of interest (ROI's) was performed using a histogram of pixel intensities where a range of values representing the density of air, ice, or soil was assigned to each ROI. Pixel intensity ranges were determined manually for each sample puck on a representative slice then automatically applied to all images in the stack. Images were segmented into between two and three ROI's (sediment/organic matter, ice, and air-filled pore space)

depending on the physical characteristics of the soil imaged. Once segmented, I applied an opening filter (erosion followed by a dilation)[35] to eliminate holes and artifacts in the ROI's attributed to noise or below the detection limits of our scanning resolution.

2.4 Image Quantification:

Using Dragonfly software, I quantified the percent composition of sediment/organic matter, ice (including surface area of ice inclusions), and air-filled pore space of each sample. Because pore space can exist below the detection limit of our instrumentation, porosity is defined as total visible porosity. Percent composition for an ROI is the total volume of a sample in voxels (1 voxel = 20 μm^3) divided by the volume of the ROI multiplied by one hundred. The surface area of ice inclusions was quantified by calculating the surface area of the ice ROI in μm^2 then normalized for puck volume because individual puck volume was slightly variable. Also, I quantified pore size distributions in equivalent diameter utilizing OpenPNM, an open-source program with wide range of pore network simulation tools[36]. Pore size classes were defined by diameter according to Brewer (1965)[37] as follows, mesopores (30-75 µm), macro very fine (75-100 µm), macro fine (1000-2000 µm), macro medium (2000-5000 µm), and macro coarse (>5000 µm). Pore connectivity using the Euler connectivity number was quantified based on pore network models made from OpenPNM. The Euler characteristic number is calculated by subtracting the redundant loops plus the number of isolated cavities from the sum of the total number of pores[7]. The more negative the Euler number, the more connected a pore matrix (for example -1000 is more connected than -100).

2.5 Physico-Chemical Analysis:

For each core, I measured gravimetric water content by mass loss[38], soil pH (Accument basic 15 pH meter Thermo Fisher Scientific, Waltham, MA, United States), and electrical

conductance (E.C) (Acument AB15 probe) by mixing ~5 grams of dry bulk soil with 25 ml of milliQ water and shaken at 150 orbits per minute on a VWR orbital shaker (Radnor, PA, United States) for 1 hour[39]. Individual scanned pucks were analyzed for total carbon and nitrogen by combustion analysis (Costech ESC 4010, Valencia, CA, United States) and gravimetric water content[38] (in addition to the bulk core measurement).

2.6 Molecular Analyses:

Soil pucks were homogenized with a sterile pestle and mortar in a walk-in freezer (~-7 ºC) at the University of New Hampshire. The pestle and mortar were sterilized with 70% ethanol between samples. From each puck ~1.5 grams of soil were co-extracted for DNA and RNA using RNeasy Power Soil Total RNA and Rneasy Power Soil DNA Elution kits (Qiagen, Germantown, MD) following manufacturer's instructions. I was unable to extract quantifiable RNA from two of the four cores from Fox, Alaska (cores two and three). After extraction, DNA and RNA was quantified using Qubit 1X dsDNA HS Assay kit and Qubit RNA HS Assay kit, respectively (Thermo Fisher Scientific, Waltham, MA). Extracted RNA was treated for any residual DNA using a DNAse 1, Rnase-free kit (Thermo Fisher Scientific, Waltham, MA) and reverse transcribed to cDNA using a High Capacity-cDNA Reverse Transcription Kit with Rnase Inhibitor kit (Thermo Fisher Scientific, Waltham, MA) following manufacturer's instructions. Extraction negative controls were included in the analysis.

Extracted DNA and cDNA were used as template DNA to amplify the V4-V5 region of the 16S rRNA gene[40]. Polymerase Chain Reactions (PCR) were run using the primers 515f (TCGTCGGCAGCGTCAGATGTGTATAAGAGACAGGTGYCAGCMGCCGCGGTAA) and 926r (GTCTCGTGGGCTCGGAGATGTGTATAAGAGACAGCCGYCAATTYMTTTRAGTTT)[41]

with Nextera adapters. For each reaction volume of 12 µl, I added 6 µl of DreamTaq hot start (green) (Thermo Fisher Scientific, Waltham, MA), 2.6 µl of H_2O solution containing 0.5 µg/µl bovine serum albumin (BSA) to reduce potential PCR inhibitors[42], 0.7 µl of 5 µM forward primer, 0.7 µl of 5 µM reverse primer, and 2 µl of template DNA or cDNA. The thermal cycling protocol was carried out with a 30 second 95℃ hot start, then 35 cycles of 30 seconds at 95˚C (denaturation), 30 seconds at 55℃ (annealing), and 60 seconds at 72℃ (extension), followed by a final step for 10 minutes at 72℃. Unique sample barcodes (Illumina Nextera DNA UD Indexes)were added in a second round of PCR sequencing (30 cycles). Sequencing took place at the University of New Hampshire Hubbard Genome Center on Illumina Novaseq 6000 (Illumina, San Diego, CA, USA).

To quantify the number of copies of 16S rRNA genes in the genomic DNA and cDNA, I ran qPCR on a Bio-Rad CFX96 (BioRad, Hercules, CA, USA) using the same primer sequences as above. Reaction volumes of 15 µl were composed of 7.5 µl Sso Advanced™ Universal SYBR® Green Supermix (BioRad, Hercules, CA, USA), 1.125 µl of 10 µM forward primer, 1.125 µl of 10 µM reverse primer, 3 µl of template gDNA, and 2.25 µl of H_2O. The thermal cycling protocol was carried out with four minutes (30 seconds for cDNA) of polymerase activation at 95℃ followed by 40 cycles of 30 seconds at 95℃ (denaturation), 30 seconds at 53℃ (annealing), 60 seconds at 72℃ (extension) according to manufacturer's instructions. Standard curves were composed of five 10-fold serial dilutions of genomic DNA from *Escherichia coli* k-12[43] and cDNA (reverse transcribed from RNA) *Escherichia coli* DH5 alpha [44] extracted from pure culture[45]. All samples and standards were run in triplicate. Samples were standardized to 0.65 ng template DNA. The reaction efficiency was > 93.5% and $R^2 > 0.99$ in all

reactions. Results were standardized to the original mass of soil and are reported as gene copies per gram soil.

2.7 Downstream processing of sequencing data:

Amplicon sequencing data was received from the University of New Hampshire Hubbard Genome Center as demultiplexed FastQ files. Any remaining adapters were removed from the reads using cutadapt[46] before ASV assignment via dada2[47]. I followed a modified version of the dada2 "big data" pipeline adapted for use with NovaSeq error rates based on recommendations from the community and developers (GitHub – ErnakovichLab/dada2_ernakovichlab). First, primers were removed from sequences using cutadapt[46] searching for both primer sequences as well as their reverse complements. At this step I also removed any reads lower than 50 bp in length. Then, in dada2 quality plots were used to assess how many base pairs to trim; forward reads were trimmed to 160 base pairs and reverse reads to 240 base pairs. Next, I binned error rates, and I compared the results of several different modified error rate learning functions on our data to find the function that worked best with NovaSeq binned quality scores. The best function was option 4 (GitHub – ErnakovichLab/dada2_ernakovichlab), which resulted in a good approximation of the observed error rates in our data. These error rates were used to assign exact sequence variants to the data. Finally, following the default dada2 pipeline, I dereplicated, removed chimeras, and assigned taxonomy using Silva db v138.

2.8 Shannon Diversity Index:

We quantified diversity using the Shannon index below where H' is the diversity index, p_i is the proportion of each species within a sample, and ln p_i is the natural logarithm of the proportion of each species within a sample[48].

$$H' = -\sum_{n=1}^{n} (pi^* \ln\ p_i)$$

Specifically, I used the R-package phyloseq[49] to calculate H' for our samples.

2.9 Statistical Analyses:

We used the R-package phyloseq[49], for downstream microbial community analyses. Prior to determining Shannon diversity and statistical analyses bacteria and archaea that were unassigned at the phylum level and chloroplasts were removed from the analysis. I then rarified all samples to a sequencing depth of 1,500 reads which represented a good balance between sequencing depth and maximizing samples available for analysis.

Differences in soil physical and chemical properties (carbon and nitrogen, pH, EC, porosity characteristics), and Shannon diversity across sites was assessed using a one-way analysis of variance (ANOVA). Due to non-normality of pore connectivity and microbial abundance data, Kruskal-Wallis analyses were used to determine differences between sites.

To explore the correlations between soil physical and chemical characteristics including pore size classes (H2) and the surface area of ice inclusions (H3), and active and total bacterial

and archaeal community abundance within sites was determined using Spearman correlations (R package 'hmisc')[50].

We used generalized linear mixed effects modeling (R package 'lme4')[51] to explore the influence of soil physical and chemical characteristics on active and total bacterial and archaeal community diversity (H1), where site was the random effect and total porosity, pore connectivity, total carbon content, and pore size classes were fixed effects. To determine the variance explained by the random effect the intraclass correlation coefficient (ICC) was used (R package 'performance')[52]. To determine which pore size classes to include in the model a separate model was run (Appendix Table 3). To determine the relationship between soil physical/chemical characteristics and active and total bacterial and archaeal community diversity within sites I used Pearson correlations (R package 'hmisc')[50].

3. RESULTS

3.1 Soil Physical Structure

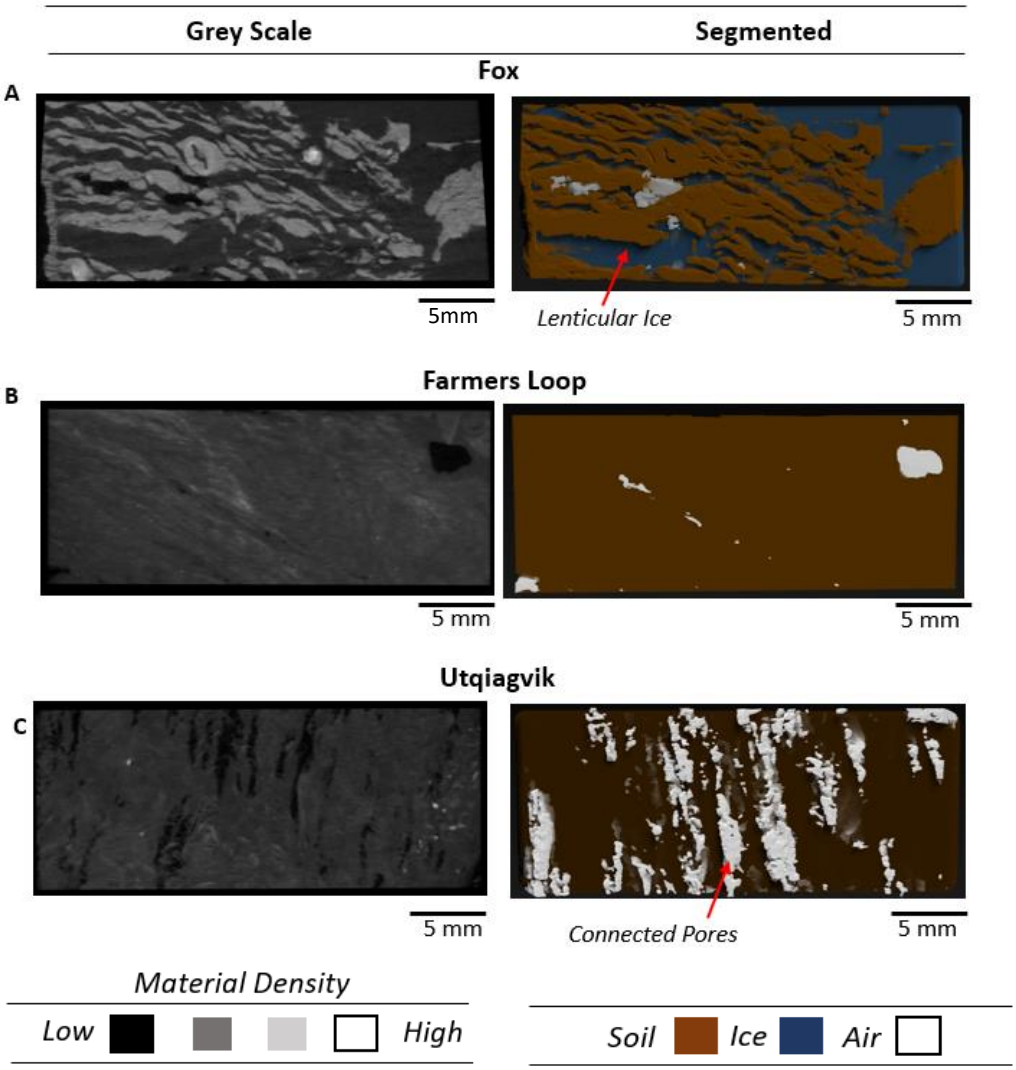

Fig. 2. Example grey scale (left) and segmented 3-dimensional cross sections (right; highlighting key features) of soil pucks displaying physical compositional differences scanned from the three study sites, A. Fox, B. Farmers Loop, C. Utqiagvik. Grey-scale images were processed and segmented for regions of interest where applicable (soil, ice, and air). Soil pucks are oriented as they were sampled from the respective core with the top nearest the top of the core. In the images on left, highest density materials appear white and lowest appear black.

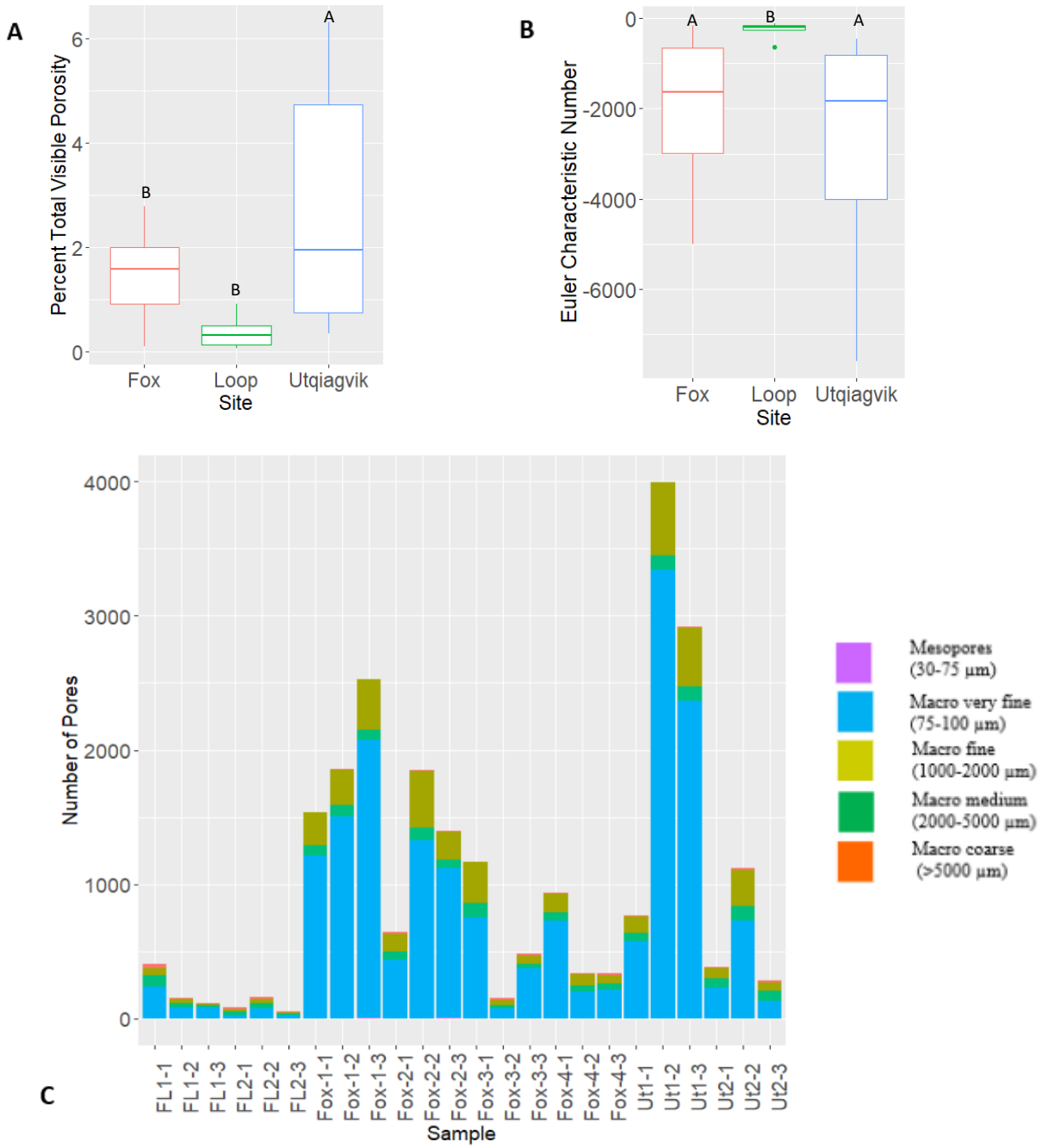

Fig. 3. ***A:*** Percent visible porosity across permafrost sites. ANOVA $p < 0.05$. Shared letters represent no significant differences. ***B:*** Pore connectivity (Euler characteristic number) across permafrost sites. A stronger negative number represents a more connected pore network. Kruskal-Wallis $p < 0.05$. Shared letters represent no significant differences. Top and bottom of boxes represent upper and lower quartiles of the data respectively, middle lines represent the median, and the top and bottom of the vertical lines represent the maximum and minimum in the data respectively. **C*:*** Distribution of pore size classes in individual permafrost pucks from the sites, as described by Brewer (1965). The sample codes (on the x-axis) have the format site name – core number – puck number. Fox, FL, and UT correspond to Fox, Farmers Loop, and Utqiagvik respectively. Pores sizes were quantified using equivalent diameter measurements.

The density of soils and the soil/ice/air structure varied greatly between sites (Fig. 2). The highest density materials, for example a quartz grains, appear as white in grey scale images while low density material such as air appears black (Fig. 2). Fox samples were dominated by lenticular ice structures which are easily distinguished from soil and air (dark grey and blue bands in the grey scale and segmented images, respectively, Fig. 2A). Farmers Loop contained very little pore space (< 1%) and did not display lenticular ice structure (Fig. 2B). Like Farmer's Loop, in Utqiagvik samples ice and soil were indistinguishable at our scanning resolution (20 μm). However, Utqiagvik had the most pore space of the three sites (Fig. 2C). While ice is typically less dense than soil, the soil at Utqiagvik and Farmers Loop displays a similar density to the density of ice at Fox likely due to high carbon and water content (Appendix A. Table 5) of the Utqiagvik and Farmers Loop soils (Fig. 2, left side). At these sites fine ice crystals result in homogenized regions of soil and ice that could not be distinguishable as separate ROIs.

Total visible porosity across sites varied from as high as 6.32% at Utqiagvik, to 0.1% at Fox, the highest mean total visible porosity at Utqiagvik (2.76%) and lowest at Farmers Loop (0.37%). Across sites total visible porosity was ~7.5 times higher at Utqiagvik than Farmers Loop (ANOVA, $p < 0.05$, Fig. 3). Fox had an intermediate level of total visible porosity and showed no significant differences with either Utqiagvik or Farmers Loop (Fig. 3A). Pore connectivity (represented as the Euler characteristic number) ranged from -7595.27 (highest connectivity) in Utqiagvik to -109.12 (lowest connectivity) in Fox. Overall, connectivity was ~10 times lower in Farmers Loop than Fox and ~18 times lower than Utqiagvik (Kruskal-Wallis, $p < 0.05$, Fig. 3B). Variance in connectivity was high within both Fox and Utqiagvik, with both sites showing an order of magnitude higher variance in connectivity than the Farmers Loop site (Fig. 3).

Across the three sites nearly all pores (> 99 %) fell within a macro classification (> 75 μm) with macro very fine pores being the most abundant pore size class on average (> 65 %) followed by macro fine pores (>17 %) (Fig. 3C). For macro very fine and macro fine pore size classes, Utqiagvik contained 394.75 and 1142.67 more pores on average than Fox and Farmers Loop (ANOVA, $p < 0.05$, Fig. 3C).

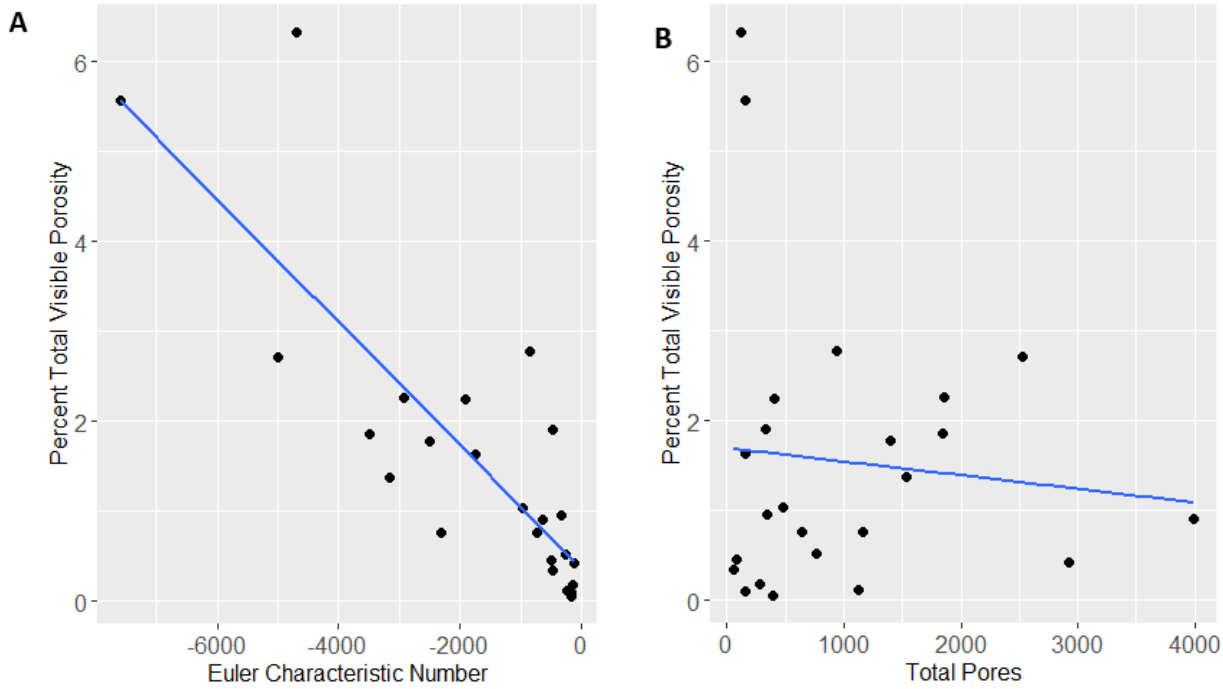

Fig. 4. ***A:*** Correlation between total visible porosity and Euler characteristic number (pore connectivity) (Pearson = -0.60, $p < 0.05$). ***B:*** Correlation between total visible porosity and total number of pores (Pearson = -0.21, $p > 0.05$).

Across samples pore connectivity and total visible porosity were significantly negatively correlated (Pearson = -0.60, $p < 0.05$, Fig. 4A). Because a more negative Euler characteristic number indicates higher pore connectivity, this demonstrates increasing pore connectivity with higher total visible porosity. Also, there was no correlation between total visible porosity and the total number of pores in a sample (Fig. 4B).

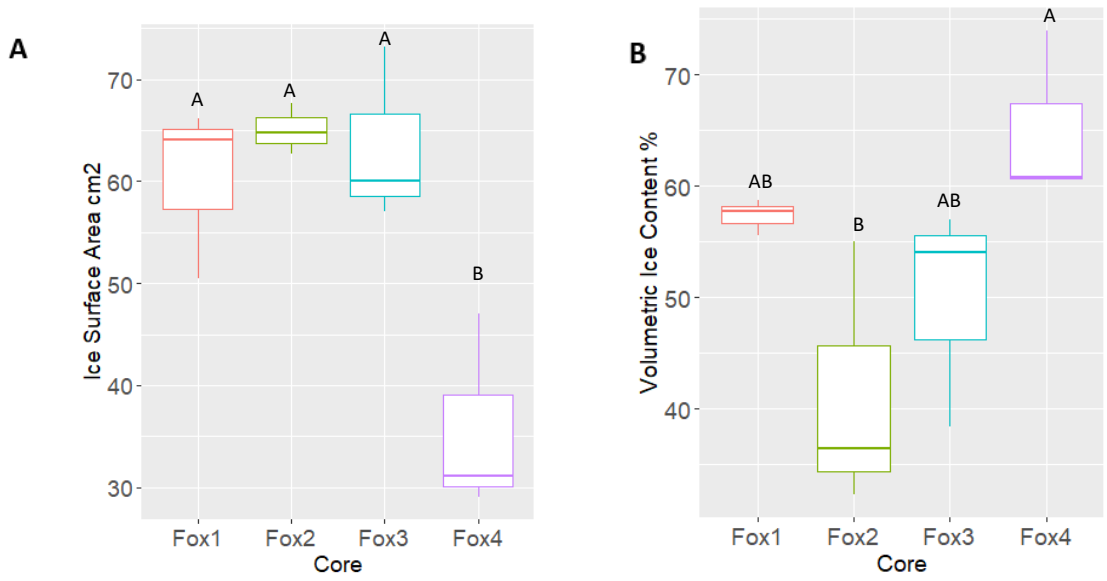

Fig 5. Ice structure in permafrost from Fox, Alaska (above the CRREL permafrost tunnel), where permafrost displays a lenticular ice structure. ***A:*** Ice inclusion surface area (cm^2) among the four cores scanned. Three pucks from each of four cores were scanned. Different letters represent significant differences (ANOVA $p < 0.05$). Boxplots are as in Fig. 3. ***B:*** Percent volumetric ice content (cm^3) normalized for sample volume among the four cores scanned in Fox, Alaska above the CRREL permafrost tunnel. Different letters represent significant differences (ANOVA $p < 0.05$). Boxplots are as in Fig. 3.

Fox was the only site displaying lenticular (non-homogenized) ice structure and here I analyzed four cores, Fox1, Fox2, Fox3, and Fox4 to investigate variation within the site. In these soils, the surface area of the ice inclusions ranged from a high of 67.7 cm^2 in Fox3 to 29.05 cm^2 in Fox4 (Fig. 5A). The ice inclusions at Fox4 had on average ~1.5 times less surface area than cores Fox1, Fox2, and Fox3 (ANOVA, $p < 0.05$, Fig. 5A). Volumetric composition of ice was more variable than ice surface area, ranging from < 42%, (Fox 2) to > 65% in Fox4, which partially contained a larger ice lens. Fox1 and Fox3 had more intermediate values, with statistical differences occurring only between Fox4 and Fox2 (ANOVA $p < 0.05$, Fig. 5B).

3.2 Soil pore structures influence on bacterial and archaeal diversity and abundance

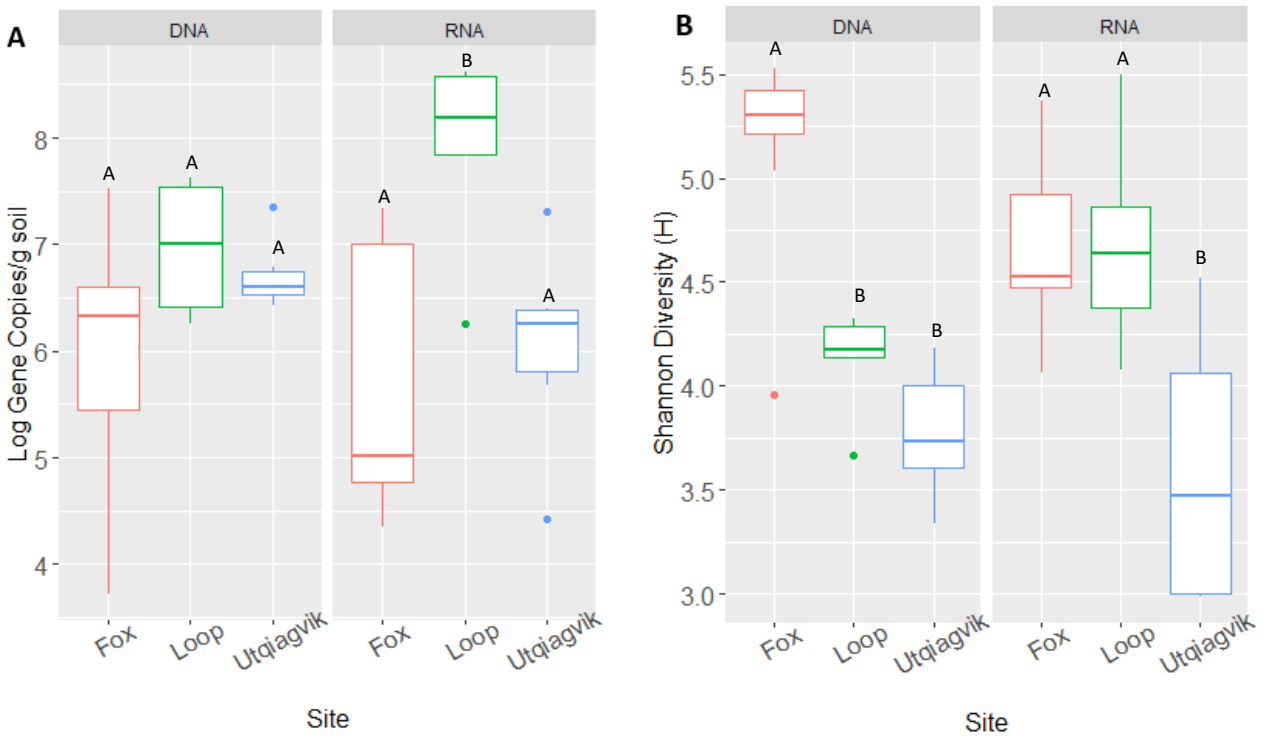

Fig 6. ***A:*** Total and active bacterial and archaeal community abundance (Log of gene copies per gram of soil) at each study site: DNA (Kruskal Wallis $p > 0.05$) RNA (Kruskal Wallis $p < 0.05$), shared letters represent no significant differences. Boxplots are as in Fig. 3.***B:*** Total and active bacterial and archaeal community Shannon diversity (H) at each study site: DNA (ANOVA $p < 0.05$), RNA (ANOVA $p < 0.05$), shared letters represent no significant differences. Boxplots are as in Fig. 3.

Despite the large heterogeneity in physical composition, abundance of the total bacterial and archaeal community (DNA gene copies) was not significantly different across study locations, although subsamples within Fox varied by several orders of magnitude (Fig. 6A). Abundance of the active bacterial and archaeal community (RNA gene copies) was significantly higher at Farmers Loop ($2.0 \times 10^8 \pm 1.8 \times 10^8$ gene copies/g soil) than Fox ($6.4 \times 10^6 \pm 9.5 \times 10^6$ gene copies/g soil) and Utqiagvik ($4.5 \times 10^6 \pm 7.9 \times 10^6$ gene copies/g soil) (Kruskal-Wallis $p < 0.05$, Fig. 6A).

Shannon diversity of the total bacterial and archaeal community was significantly higher at Fox ($H = 5.2 \pm 0.4$) than Farmers Loop ($H = 4.1 \pm 0.2$) and Utqiagvik ($H = 3.8 \pm 0.3$)

(ANOVA $p < 0.05$, Fig. 6B). The Shannon diversity of the active bacterial and archaeal community at both Fox (4.7 ± 0.5) and Farmers Loop (4.7 ± 0.5) were significantly higher than Utqiagvik (3.6 ± 0.7) (ANOVA $p < 0.05$, Fig. 6B).

To determine which, if any, soil structural and physico-chemical characteristics influenced Shannon's bacterial and archaeal diversity for both the active and total communities, I ran generalized linear mixed effects models. For the active bacterial and archaeal communities neither pore characteristics nor total carbon content were related to Shannon diversity, but the random effect of site accounted for most of the variance in Shannon diversity (ICC = 0.69, Table 1).

Table 1. Estimate and standard error for each explanatory variable from mixed model analyses explaining the variance in Shannon diversity of the bacterial and archaeal communities. Intraclass correlation coefficient (ICC) accounts for the variance explained by the random effect, site. The model is as follows, model > lmer (diversity~ C + Connectivity + Visible.Porosity + Macro.Fine +(1|Site).

Active Community	**Pore Connectivity**	**Visible Porosity**	**Total Carbon**	**Macro Fine Pores**
Estimate	-0.03	-0.03	0.38	-0.16
Standard Error	0.45	0.44	0.43	0.21
P-Value	0.94	0.94	0.42	0.48
		ICC = 0.69		
Total Community	**Pore Connectivity**	**Visible Porosity**	**Total Carbon**	**Macro Fine Pores**
Estimate	-0.19	-0.39	-0.06	0.02
Standard Error	0.14	0.14	0.21	0.09
P-Value	0.17	0.01	0.77	0.85
		ICC = 0.834		

Like the active community, Shannon diversity of the total community was highly variable among sites (ICC = 0.83, Table 1). However, in contrast to the active community, pore connectivity had a marginal negative relationship with Shannon diversity of the total community (Est. = -0.19, S.E = 0.14, Table 1) and total visible porosity had a significant negative relationship with total community diversity (Est. = -0.39, S.E = 0.14, $p < 0.05$, Table 1).

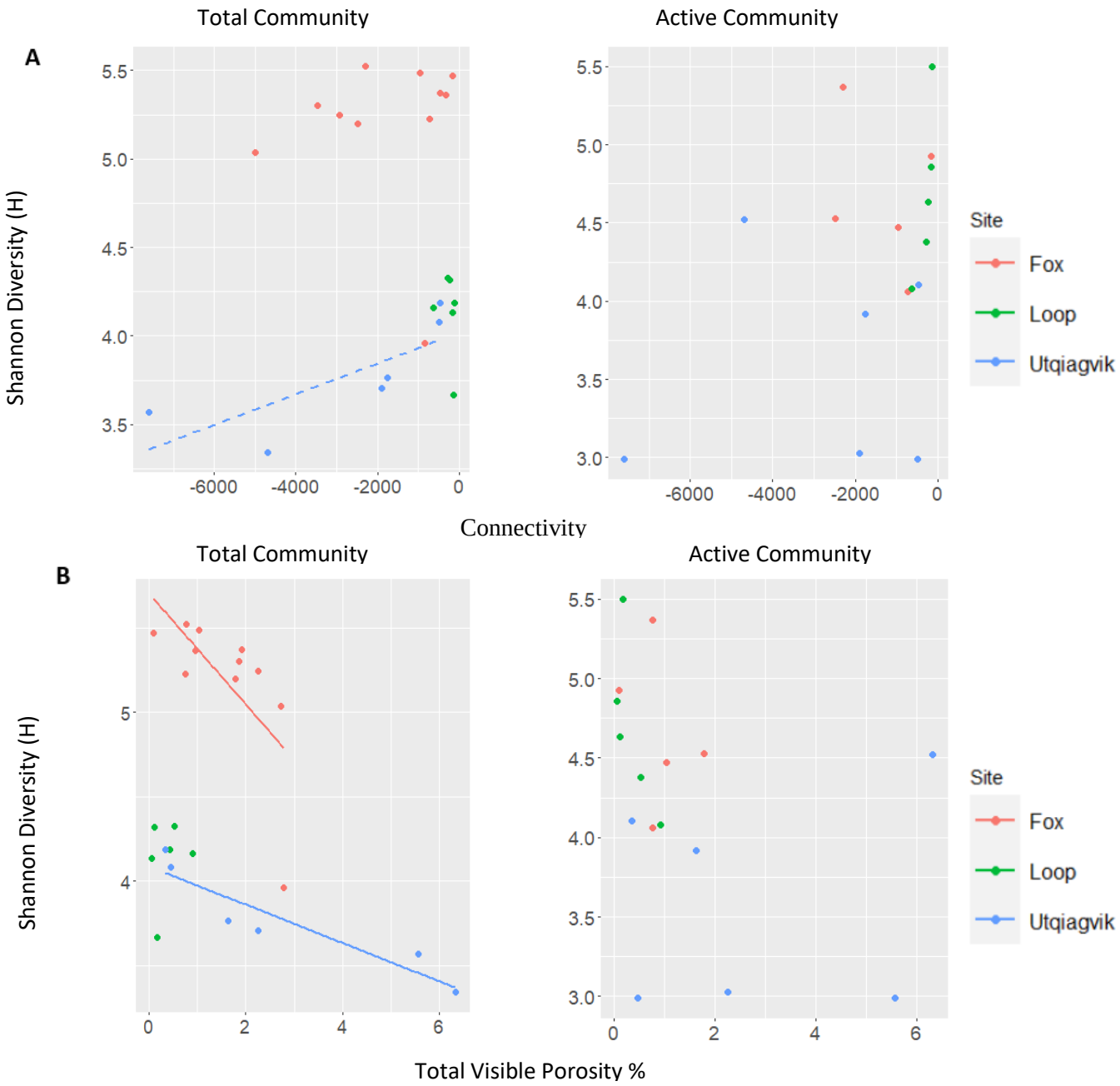

Fig 7. ***A:*** Correlations between pore connectivity (high connectivity indicated by a strong negative number) and Shannon diversity index of the total and active bacterial and archaeal communities at Fox (Active, Pearson = -0.33, $p > 0.05$. Total, Pearson = 0.02, $p > 0.05$), Utqiagvik (Active: Pearson = 0.08, $p > 0.05$. Total: Pearson = 0.77, $p = 0.073$), and Farmers Loop (Active, Pearson = 0.79, $p > 0.05$. Total, Pearson = -0.22, $p > 0.05$). Solid and dashed lines denote significant ($p < 0.05$) or nearly significant (p 0.05-0.10) respectively. ***B:*** Correlations between total visible porosity and Shannon diversity index of the total and active bacterial and archaeal communities at Fox (Total, Pearson = -0.66, $p < 0.05$. Active, Pearson = -0.30, $p > 0.05$), Utqiagvik (Total: Pearson = -0.93, $p < 0.05$. Active: Pearson = 0.19, $p > 0.05$), and Farmers Loop (Total, Pearson = 0.23, $p > 0.05$. Active, Pearson = -0.74, $p > 0.05$). Solid and dashed lines denote significant ($p < 0.05$) or nearly significant (p 0.05-0.10) respectively.

Because the variation in the relationship between soil physical structure and diversity was large among sites, I investigated the correlation between soil physical characteristics and diversity within each site individually. At Fox and Farmers Loop, pore connectivity (high connectivity indicated by a strong negative number) had no correlation to the Shannon diversity of the total bacterial and archaeal community (Fig. 7A). At Utqiagvik there was a nearly significant positive relationship between connectivity and diversity of the total bacterial and archaeal community or as connectivity decreased, diversity increased (Pearson = 0.77, $p = 0.073$, Fig. 7A). At Farmers Loop and at Fox there was no significant correlation between pore connectivity and diversity of the active bacterial and archaeal community (Fig. 7A), however RNA was not recoverable from cores two and three at Fox. Additionally, the active community at Utqiagvik had no significant correlation with pore connectivity (Fig. 7A).

Fox and Utqiagvik displayed a strong negative correlation between total visible porosity and diversity of the total community (Pearson = -0.66, $p < 0.05$, Pearson = -0.93, $p < 0.05$, Fig. 7B). Farmers Loop had no correlation between total visible porosity and diversity of the total community (Fig. 7B), however the variation in visible porosity was low. In contrast to the total community, there were no correlations between active community diversity and total visible porosity at any site (Fig. 7B).

4. DISCUSSION

4.1 Micro-CT scanning of permafrost is effective for quantifying macroporosity, but has methodological limitations preventing finer resolution quantification

In this study I utilized micro-CT scanning to quantify structures in frozen permafrost soil where scanning has been used mostly to quantify features on a macro-scale (> 100 µm). I was able to achieve the quantification of pore and ice structures down to 72 µm and found that permafrost generally has lower macroporosity than temperate soils. Few studies have investigated the volumetric composition of intact pore space in frozen permafrost utilizing micro-CT scanning[28,30]. I generally expected our samples to exhibit higher porosity than previous studies in permafrost[28,30] because our scanning resolution (20 µm) was 2.5 to 10 times higher, and only pores larger than scanning resolution can be quantified[6]. I also expected porosity to be lower than that of unfrozen soil. While at a base level, soil particle size sets a lower-bound on microporosity, i.e., coarse sand is more porous than fine clay or even silt[53], many other abiotic and biotic properties contribute to soil porosity. For example, porosity is influenced by the formation and distribution of soil aggregates whose inter aggregate pore space can influence soil transport of water and air[54]. In addition, pores left behind by biological activity (bio-pores) from macro invertebrates and plant roots can add to the overall porosity of the soil[55]. However, frozen permafrost soil is subject to much less and slower physical and biological disturbance[56] which likely leads to lower porosity.

In this study the average total visible porosity was low (Fox = 1.53%, Farmers Loop = 0.37%, Utqiagvik = 2.76%) (Fig. 3A) compared to temperate soils which can exhibit significantly higher porosity[1,6,7]. Calmels & Allard (2004) found total visible porosity to average 2.3% in permafrost samples at a resolution of 200 µm. Similarly, Nitzbon et al. (2022) observed

an average total visible porosity of 2-3% at a resolution of 50 μm, as well as occasional higher total visible porosity (~ 8 %) correlated with excess ice content. Although our scanning resolution was 20 μm, I was limited by our ability to make inferences about pores smaller than ~75 μm (e.g., meso- and micropores). Practically, the smallest objects that can be identified are two to three times larger than the scanning resolution[30,57]. In order to maintain sample integrity (i.e., to restrict thawing, which would change the physical composition of the sample), I had to use short scan times (~20 minutes). Although the scanning took place in a cold room at-10ºC, the cavity of the scanner itself would eventually rise above freezing thus restricting scan time which contributed to noise and associated limitations in resolution.

In contrast to permafrost soil, pore space has been studied extensively in unfrozen soils where there are fewer methodological limitations to scan time. In unfrozen systems Lucas et al. (2019), Shein et al. (2015), and Bouchaert et al. (2013) achieved resolutions of 5 μm, 8.75 μm, and 9.44 μm and total visible porosities of 23.7 to 35.6%, 3.9 to 6.8%, and 13.2% respectively, demonstrating that our porosities fall below total visible porosity percentages observed in some studies with much higher resolution. However, despite limitations in detection, the most prevalent pore size classes I quantified are relatively concurrent with studies from temperate soils. In soddy-podzolic silt loamy soils, macro very fine pores (75 -1000 μm) were the most abundant in soil samples at a scanning resolution of 8.75 μm[6]. Similarly, in a conglomerate soil from an open cast coal mine area, with a scanning resolution of 30 μm, macro very fine pores (75 -1000 μm)were the most abundant across a wide range in bulk densities, although mesopores (30-75 μm) were also highly abundant[58]. This may indicate that the higher porosity detected in temperate soil studies is mainly due to real differences in porosity rather than our limitations and

that pores falling within the mesopore class (~30-75 μm) generally make up a relatively smaller percentage of the pore space in soils compared to macro/microporosity.

In addition, regardless of the scanning resolution, micro-CT underestimates pore space because the majority of micropore space falls below the detection limit or resolution. Even in unfrozen soils with high scanning resolutions (>5 μm and <10 μm)[1,6,7] pores are abundant below 5 μm but cannot be quantified. Micropores account for the majority of the total pore space in unfrozen soil, and most soils have a total porosity between 30-70%[59]. This methodological limitation of micro-CT can be managed because micropores are strongly correlated to macropores in some soils[58]. Even if microporosity is considered based on an assumed relationship with macroporosity, it is likely permafrost is less porous than unfrozen soils.

Even at low porosities, Euler connectivity was sensitive enough to detect high variability in pore connectivity between samples with Utqiagvik and Fox sites exhibiting higher connectivity than Farmers Loop (Fig 3B). Pore connectivity via the Euler characteristic number has not been quantified in permafrost soils but is an effective tool for analyzing unfrozen soil pore structure[7,58]. Overall, there was a strong negative correlation (Fig. 4A) between total visible porosity and Euler connectivity, or as total visible porosity increased so did Euler connectivity. The same relationship between porosity and connectivity has also been observed in studies of unfrozen soils, for example in agricultural and conglomerate open cast coal mine soils[7,58], but in some agricultural systems, there is no relationship between the two[4,60]. This may occur when an increase in porosity is a function of more or larger isolated pores increasing porosity but not connectivity.

4.2 Quantifying pore ice in permafrost is not feasible in high carbon and water content soils without higher resolution scanning

We observed lenticular ice structures in only one site, Fox and found considerable variability among cores. Quantifying ice structure in the high organic matter sites, Farmers Loop and Utqiagvik, was not feasible as ice and ice filled pores could not be distinguished from soil which is composed of homogenized mineral, organic, and ice material. This is likely because both ice and organic matter—which contains high amounts of water (or ice)—are both low-density and result in similar intensities during CT-scanning[61]. Thus, distinguishing ice filled pores, ice features, and isolated organic matter may only be possible in mineral-dominated permafrost or with very high-resolution scanning not currently achieved by permafrost scanning studies to date or possible with current methods.

Fox contained ice features which I classify as lenticularly layered cryostructures, as previously described by Bray et al. (2006) (Fig 5A). I quantified the surface area of this ice matrix. One of the four cores (Fox4) had significantly lower ice surface area than the other three (Fig. 5A) because the pucks from Fox 4 were drilled at the interface of a large ~2 cm thick ice lens that did not affect the other cores. Ice surface area was low among subsamples in Fox4 because some of this ice lens was extracted as part of the subsamples (solid ice has much less surface area than a matrix of ice in the same volume). Also, I found volumetric ice content to range from 41% in Fox2 to > 65% in Fox4 (the core with a large ice lens) (Fig. 5B). Similarly, Nitzbon et al. (2022) and Camels and Allard (2004) found volumetric ice content spanning ~20 to >97% and ~40 to 80%, respectively. The heterogeneity in volumetric ice content of subsamples only millimeters apart was as high as ~23% in Fox2, ~15% in Fox3, and ~14% in Fox 4 (Fig. 5B). It is possible that the detection limits of the instrument limited our quantification

of smaller ice structures (< 75 μm). However, the formation of lenticular structured soil results in dried mineral interlayers and relatively large ice features[9]. Also, Nitzbon et al. (2022) compared lab measurements of volumetric ice content to micro-CT quantification and found CT measurements to be off by 10-20% in ice rich samples and greater than 20% in sediment rich samples. Considering that the Fox samples had high ice content in lenticular structures, and our increased resolution (20 μm), I assume our scanning was relatively comprehensive in its ability to quantify volumetric ice content.

4.3 Macroporosity is a driver of microbial community diversity

Soil pores may be important for explaining microbial community dynamics in permafrost. Pores influence the availability and distribution of unfrozen water, likely dictating the activity and abundance of metabolically active microbes in the soil. Also, pore connectivity is an important force governing microbial diversity in unfrozen soils[18,19], where diversity in soils tends to increase with a decrease in pore connectivity[18–20]. In addition to pores, the area surrounding ice inclusions in permafrost may represent potentially habitable space for active microbes. However, while theoretically plausible, it is unclear if these mechanisms are at play in permafrost soil.

Our findings did not support our hypothesis that pore connectivity of air-filled pore networks would influence the diversity of the active bacterial and archaeal communities across sites (Table 1). One possible explanation for this result is that RNA may not be the best representation of the active fraction of the microbial community due to varying life history strategies among permafrost taxa and the likelihood of permafrost harboring a high quantity of dormant cells[62] which may contain high quantities of RNA[63]. Also, obtaining high yields of RNA from nucleic acid extractions of environmental samples like permafrost which has low biomass

and microbial activity can be difficult[64]. RNA yields from this study were comparable to that of DNA yields, and even greater in some samples, but for more than half of the Fox samples I was unable to extract any RNA despite multiple efforts. Considering the close proximity of these cores, randomized extraction design, and similar physico-chemistry, I am uncertain why these samples exhibited no quantifiable RNA. Thus, using RNA to detect the influence of pore connectivity on diversity may be hindered by our ability to accurately capture the diversity of the active community.

In contrast to RNA, which may only reflect the active community at a single point in time, DNA represents the active, dormant, and dead members of the bacterial and archaeal community[65] and the diversity of this community may better reflect the influence of soil structure over longer time scales. In the total bacterial and archaeal community I saw limited evidence of the inverse relationship between diversity and connectivity proposed and demonstrated by other studies[18–20]. Although there was no relationship between pore connectivity and total community diversity across sites (Table 1), the most porous site, Utqiagvik, showed a nearly significant ($p < 0.1$) decreasing trend in diversity as connectivity increased, aligning with our hypothesis (Fig 7A). However, the other two sites did not show this relationship, suggesting that the trend often observed in temperate systems[18–21] may not hold in permafrost soils. Instead, I saw that total visible porosity was the most influential factor explaining diversity of the total bacterial and archaeal community, indicating that diversity decreased with increased porosity. The most porous sites displayed this relationship while Farmers Loop, which contained almost no detectable pore space, did not (Fig. 7B).

We saw that in contrast to our first hypothesis macroporosity, not pore connectivity, was a driver of microbial diversity in permafrost soils. This result may indicate that total porosity is a

better indicator of soil connectivity when considering only macropores like in our study. In unfrozen soils macropores can connect water and air to surrounding meso and micropores, thus an increase in macropore space may better indicate connectivity than a measure like the Euler number, which may not reflect microbial-relevant connectivity accurately as only applied to visible pores. Regardless, porosity and connectivity often co-occur, both in this study and others[7,58], where increasing porosity is positively correlated with connectivity (Fig. 4A) so these two characteristics may reflect similar effects on microbial communities.

Numerous studies have demonstrated that connectivity and diversity have an inverse relationship[18,19,21]. However, in permafrost it might be expected this relationship is a positive where microbial community diversity increases with increases in connectivity because macropores are not hydrologically connected and should act as geographical barriers creating dysconnectivity within the soil ecosystem. Yet our results contradict this mechanism and display an inverse relationship, suggesting pores in permafrost are functioning like in unfrozen soil, although this is unlikely due to the lack of available unfrozen water in macropores restricting any hydrological connection. Thus, a more realistic explanation is that I are observing the legacy of soil pore structure effects on diversity from prior to the soils transition to a frozen state. Due to thermodynamic restraints, the inhibition of dispersal is a key factor structuring community composition throughout permafrost[66]. As a result, the current spatial distribution of diversity observed in our samples could reflect the influence of pore structure from when the permafrost entered its frozen state. The relationship I see between diversity and connectivity in permafrost is that of an unfrozen soil. Also, I could be observing the true diversity of the soil being masked by relic DNA, or DNA from microbes that are no longer present within the soil community, which can persist for thousands of years in permafrost due to low temperatures and microbial

activity[67,68]. However, unlike temperate soils where relic DNA has been shown to obscure accurate characterization of microbial communitites[45], in permafrost relic DNA has been demonstrated to not significantly alter microbial community composition[62]. In addition to inhibition of dispersal, the null effect of relic DNA provides further evidence that current permafrost microbial communities reflect past conditions which would include any influence of pore structure. Thus, despite the evidence that pore structure is not shaping diversity in situ, it should still be considered among the factors influencing the spatial heterogeneity of microbial community structure in permafrost soils.

4.4 Pore size classes and ice surface area did not influence active microbial abundance

Our second hypothesis which stated that soil with an increased abundance of larger pores, which are uninhabitable because they are too large to sustain liquid water, will exhibit lower bacterial and archaeal abundance, was not supported. I saw that pore size classes did not correlate with the abundance of the active the bacterial and archaeal community within each site (Appendix Table 1). Despite our ability to quantify pore size classes spanning an order of magnitude in diameter, these variously-sized macropores—whether they are 75 or 1000 μm—likely function similarly because they contain little to no liquid water at freezing temperatures[23]. As a result, I also questioned if total pore abundance correlated with active microbial abundance since an increased number of uninhabitable pores could potentially decrease habitable space in the soil. However, there were no significant relationships with the total abundance of pores (Appendix Table 1). In part this is likely because increased numbers of pores did not translate to increased total porosity or samples with more pores also often had smaller pores (Fig. 4B), which also had no correlation with the active bacterial and archaeal abundance (Appendix Table 1). Similarly, within Fox there were no significant correlations between the surface area of ice

inclusions and active bacterial and archaeal abundance, a finding counter to our third hypothesis that ice surface area provides an 'oasis' of liquid water leading to increases in microbial abundance (Appendix Table 2). Again, using RNA for a proxy of active microbial abundance may not be comprehensive which could explain these results. Additionally, unfrozen water may persist beyond the neighborhoods of ice inclusions within small pores. However, significant unfrozen water is unlikely beyond these areas due to the drying effect during formation of lenticularly structured permafrost[9] and the sandy texture which makes the persistence on unfrozen water in pores low[10]. While the absence of any relationships between active microbial abundance and ice surface area may have a biological explanation, I do not have sufficient evidence to draw conclusions as ice inclusions were only present in one site. However, there is still strong evidence that ice and other structural characteristics of permafrost directly influence the availability and distribution of liquid and active microbial abundance[9,25]. Thus, to capture these relationships, direct measurements of unfrozen liquid water content through high-field 2H NMR[69] are needed to accompany more sensitive, high resolution structural and microbial data.

5. CONCLUSIONS

Micro-CT scanning is an effective tool to quantify macro scale features in permafrost soil, including porosity, connectivity, pore size distribution, and ice structure (>75 μm). However, due to the constraints on scanning time caused by the heat generated by the scanning instrument, quantifying relevant micro and meso-structures (<75 um) is still beyond the capabilities of current micro-CT permafrost studies. To address this challenge a micro-CT setup capable of maintaining sub-freezing temperatures for a prolonged period (e.g., > 1 hour) is needed. Despite limitations to the scanning resolution, I found permafrost soil to be generally less porous than temperate soil while sharing commonalities like the dominant pore size classes and the positive correlation between connectivity and porosity.

I was able to identify macroporosity as a driver of microbial diversity and provide evidence that microbial communities display little dispersal under permafrost conditions, which may help explain the current spatial distribution of diversity observed. Also, despite strong evidence in the literature suggesting soil structure and its influence on unfrozen water should affect the abundance of the active microbial community, I saw no relationship between microbial abundance and pore or ice structure. Effectively quantifying the influence of permafrost structure on microbial abundance will require quantification of structures on the micro scale (<30 μm), providing a more comprehensive view of features influencing unfrozen water distribution in addition to more sensitive microbial analyses.

APPENDIX A.

Table 1. Spearman correlations between active bacterial and archaeal abundance and pore size classes, porosity, and total pores at the three study sites Fox, Utqiagvik, and Farmers Loop. Significant P value denoted with *.

	Fox	Utqiagvik	Farmers Loop
Visible Porosity	0.20	0.43	-0.60
Macro Very Fine	-0.50	0.54	0.30
Macro Fine	-0.60	-0.03	0.30
Macro Medium	-0.60	0.03	0.20
Macro Coarse	-0.40	0.64	-0.20
Total Pores	-0.50	0.37	0.30
Total Carbon	0.60	0.71	0.80
Water Content	-0.30	0.49	0.80

Table 2. Spearman Correlations between active and total bacterial and archaeal abundance, ice surface area (cm^2) and percent volumetric composition of ice Fox. Significant P value denoted with *.

	Active	Total
Ice Content	0.70	-0.48
Ice Surface Area	-0.60	0.09

Table 3. Spearman correlations between total bacterial and archaeal community abundance and physico-chemical variables of interest. Significant P value denoted with *.

	Fox	***Utqiagvik***	***Farmers Loop***
Visible Porosity	-0.51	-0.31	0.77**.**
Macro Very Fine	-0.25	0.26	0.37
Macro Fine	-0.18	0.6	0.37
Macro Medium	-0.34	0.55	0.26
Macro Coarse	-0.05	0.12	-0.26
Total Pores	-0.24	0.31	0.37
Total Carbon	0.15	-0.26	-0.37
Gravimetric Water Content	-0.37	-0.37	-0.36
Percent Volume of Ice	-0.48	N/A	N/A
Ice Surface Area	0.09	N/A	N/A

Table 4. Estimate and standard error for pore size classes from mixed model analyses explaining the variance in Shannon diversity of the bacterial and archaeal communities. The model is as follows, model > lmer (diversity~ Macro.Fine + Macro.Medium + Macro.Coarse +(1|Site).

Active Community	**Macro Fine**	**Macro Medium**	**Macro Coarse**
Estimate	-0.61098	-0.09342	0.20132
Standard Error	0.99457	0.88557	0.60715
Total Community			
Estimate	0.4518	-0.3944	0.2349
Standard Error	0.5877	0.5144	0.3559

Table 5. Average total percent carbon, total percent nitrogen, volumetric water content, pH, and electric conductivity ± standard deviation measured at the 3 study sites Fox, Farmers Loop, and Utqiagvik, Alaska.

	Fox	**Farmers Loop**	**Utqiagvik**
%Carbon	2.14±1.20	38.75± 1.48	26.07± 10.88
%Nitrogen	0.12±0.05	2.03±0.18	1.36±0.59
%Water Content	57.65±11.40	78.20±2.03	69.23±6.80
pH	4.72±0.01	4.97±0.12	4.29±0.18
E.C	414.85±37.83	287.33±55	254.2±67.80

LIST OF REFERENCES

1. Bouckaert L, Sleutel S, Van Loo D, et al. Carbon mineralisation and pore size classes in undisturbed soil cores. *Soil Res*. 2013;51(1):14-22. doi:10.1071/SR12116

2. Mangalassery S, Sjögersten S, Sparkes DL, Sturrock CJ, Mooney SJ. The effect of soil aggregate size on pore structure and its consequence on emission of greenhouse gases. *Soil Tillage Res*. 2013;132:39-46. doi:10.1016/j.still.2013.05.003

3. Kravchenko AN, Guber AK. Soil pores and their contributions to soil carbon processes. *Geoderma*. 2017;287:31-39. doi:10.1016/j.geoderma.2016.06.027

4. Gao L, Becker E, Liang G, et al. Effect of different tillage systems on aggregate structure and inner distribution of organic carbon. *Geoderma*. 2017;288:97-104. doi:10.1016/j.geoderma.2016.11.005

5. Munkholm LJ, Heck RJ, Deen B. Soil pore characteristics assessed from X-ray micro-CT derived images and correlations to soil friability. *Geoderma*. 2012;181-182:22-29. doi:10.1016/j.geoderma.2012.02.024

6. Shein E V., Skvortsova EB, Dembovetskii A V., Abrosimov KN, Il'in LI, Shnyrev NA. Pore-size distribution in loamy soils: A comparison between microtomographic and capillarimetric determination methods. *Eurasian Soil Sci*. 2016;49(3):315-325. doi:10.1134/S1064229316030091

7. Lucas M, Schlüter S, Vogel HJ, Vetterlein D. Soil structure formation along an agricultural chronosequence. *Geoderma*. 2019;350(April):61-72. doi:10.1016/j.geoderma.2019.04.041

8. Schipper LA, Hobbs JK, Rutledge S, Arcus VL. Thermodynamic theory explains the temperature optima of soil microbial processes and high Q10 values at low temperatures. *Glob Chang Biol*. 2014;20(11):3578-3586. doi:10.1111/gcb.12596

9. Ostroumov VE, Siegert C. EXOBIOLOGICAL ASPECTS OF MASS TRANSFER IN MICROZONES OF PERMAFROST DEPOSITS. 1996;18(12):79-86.

10. Gilichinsky DA, Rivkina EM. Permafrost microbiology. *Encycl Earth Sci Ser*. 2011;6(9781402092114):726-732. doi:10.1007/978-1-4020-9212-1_162

11. Leewis MC, Berlemont R, Podgorski DC, et al. Life at the Frozen Limit: Microbial Carbon Metabolism Across a Late Pleistocene Permafrost Chronosequence. *Front Microbiol*. 2020;11(July):1-15. doi:10.3389/fmicb.2020.01753

12. Strong DT, De Wever H, Merckx R, Recous S. Spatial location of carbon decomposition in the soil pore system. *Eur J Soil Sci*. 2004;55(4):739-750. doi:10.1111/j.1365-2389.2004.00639.x

13. Bronick CJ, Lal R. Soil structure and management: A review. *Geoderma*. 2005;124(1-2):3-22. doi:10.1016/j.geoderma.2004.03.005

14. Lugato E, Morari F, Nardi S, Berti A, Giardini L. Relationship between aggregate pore size distribution and organic-humic carbon in contrasting soils. *Soil Tillage Res*.

2009;103(1):153-157. doi:10.1016/j.still.2008.10.013

15. Liang A, Zhang Y, Zhang X, et al. Investigations of relationships among aggregate pore structure, microbial biomass, and soil organic carbon in a Mollisol using combined non-destructive measurements and phospholipid fatty acid analysis. *Soil Tillage Res*. 2019;185(August 2018):94-101. doi:10.1016/j.still.2018.09.003

16. Paradelo M, Katuwal S, Moldrup P, Norgaard T, Herath L, de Jonge LW. X-ray CT-Derived Soil Characteristics Explain Varying Air, Water, and Solute Transport Properties across a Loamy Field. *Vadose Zo J*. 2016;15(4):vzj2015.07.0104. doi:10.2136/vzj2015.07.0104

17. Lucas M, Vetterlein D, Vogel HJ, Schlüter S. Revealing pore connectivity across scales and resolutions with X-ray CT. *Eur J Soil Sci*. 2021;72(2):546-560. doi:10.1111/ejss.12961

18. Heijnen C. A determination of protective microhabitats for bacteria introduced into soil. *FEMS Microbiol Lett*. 1991;85(1):73-80. doi:10.1016/0378-1097(91)90633-l

19. Carson JK, Gonzalez-Quiñones V, Murphy D V., Hinz C, Shaw JA, Gleeson DB. Low pore connectivity increases bacterial diversity in soil. *Appl Environ Microbiol*. 2010;76(12):3936-3942. doi:10.1128/AEM.03085-09

20. Chau JF, Bagtzoglou AC, Willig MR. The Effect of Soil Texture on Richness and Diversity of Bacterial Communities. *Environ Forensics*. 2011;12(4):333-341. doi:10.1080/15275922.2011.622348

21. Xia Q, Zheng N, Heitman JL, Shi W. Soil pore size distribution shaped not only compositions but also networks of the soil microbial community. *Appl Soil Ecol*. 2022;170(April 2021):104273. doi:10.1016/j.apsoil.2021.104273

22. Or D, Wraith JM, Warrick AW. Soil water content and water potential relationships. *Soil Phys companion*. 2002;1:49-84.

23. Drotz SH. *Biogeochemical Processes in Frozen Soils*.; 2010.

24. Atkins P, De Paula J. *Physical Chemistry*. Macmillan; 2002.

25. Harrysson S, Tilston EL, Sparrman T, Schleucher J, Nilsson M, Öquist MG. Geoderma Contributions of matric and osmotic potentials to the unfrozen water content of frozen soils. *Geoderma*. 2009;148(3-4):392-398. doi:10.1016/j.geoderma.2008.11.007

26. Kirkham MB. *Principles of Soil and Plant Water Relations*. Elsevier Science; 2014. https://books.google.com/books?id=Y5r8AgAAQBAJ

27. Bray MT, French HM, Shur Y. Further cryostratigraphic observations in the CRREL permafrost tunnel, Fox, Alaska. *Permafr Periglac Process*. 2006;17(3):233-243. doi:10.1002/ppp.558

28. Calmels F, Allard M. Ice segregation and gas distribution in permafrost using tomodensitometric analysis. *Permafr Periglac Process*. 2004;15(4):367-378. doi:10.1002/ppp.508

29. Calmels F, Clavano WR, Froese DG. Progress on X-ray computed tomography (CT) scanning in permfrost studies. *63rd Can Geotech Conf 6th Can Permafr Conf*. Published online 2010:1353-1358.

30. Nitzbon J, Gadylyaev D, Schlüter S, Köhne JM, Grosse G, Boike J. Brief communication : Unravelling the composition and microstructure of a permafrost core using X-ray computed tomography. 2022;(April):1-13.

31. Mangalassery S, Sjögersten S, Sparkes DL, Sturrock CJ, Mooney SJ. The effect of soil aggregate size on pore structure and its consequence on emission of greenhouse gases. *Soil Tillage Res*. 2013;132:39-46. doi:10.1016/j.still.2013.05.003

32. Meira Cássaro FA, Posadas Durand AN, Gimenez D, Pedro Vaz CM. Pore-Size Distributions of Soils Derived using a Geometrical Approach and Multiple Resolution MicroCT Images. *Soil Sci Soc Am J*. 2017;81(3):468-476. doi:10.2136/sssaj2016.09.0291

33. Boas FE, Fleischmann D. CT artifacts: causes and reduction techniques. *Imaging Med*. 2012;4(2):229-240.

34. Chambolle A. An Algorithm for Total Variation Minimization and Applications. *J Math Imaging Vis*. 2004;20(1-2):89-97. doi:10.1023/B:JMIV.0000011321.19549.88

35. Haralick RM, Sternberg SR, Zhuang X. Image analysis using mathematical morphology. *IEEE Trans Pattern Anal Mach Intell*. 1987;(4):532-550.

36. Gostick J, Aghighi M, Hinebaugh J, et al. OpenPNM: a pore network modeling package. *Comput Sci Eng*. 2016;18(4):60-74.

37. Brewer R. Fabric and mineral analysis of soils. *Soil Sci*. 1965;100(1):73.

38. Gardner WH. Water content. Methods of soil analysis: Part 1. Physical and mineralogical properties, including statistics of measurement and sampling, ed. *CA Black Am Soc Agron Madison, Wisconsin*. 1983;82:127.

39. Rayment GE, Higginson FR. *Australian Laboratory Handbook of Soil and Water Chemical Methods.* Inkata Press Pty Ltd; 1992.

40. Klindworth A, Pruesse E, Schweer T, et al. Evaluation of general 16S ribosomal RNA gene PCR primers for classical and next-generation sequencing-based diversity studies. *Nucleic Acids Res*. 2013;41(1):1-11. doi:10.1093/nar/gks808

41. Parada AE, Needham DM, Fuhrman JA. Every base matters: Assessing small subunit rRNA primers for marine microbiomes with mock communities, time series and global field samples. *Environ Microbiol*. 2016;18(5):1403-1414. doi:10.1111/1462-2920.13023

42. Kreader A. C. Relief of amplification inhibition in PCR with bovine serum albumin or T4 Gene 32 Protein. *Appl Environ Microbiol*. 1996;62(3):1102-1106.

43. Blattner FR, Plunkett G, Bloch CA, et al. The complete genome sequence of Escherichia coli K-12. *Science (80-)*. 1997;277(5331):1453-1462. doi:10.1126/science.277.5331.1453

44. Chen J, Li Y, Zhang K, Wang H. Whole-genome sequence of phage-resistant strain Escherichia coli DH5α. *Genome Announc*. 2018;6(10):e00097-18.

45. Carini P, Marsden PJ, Leff JW, Morgan EE, Strickland MS, Fierer N. Relic DNA is abundant in soil and obscures estimates of soil microbial diversity. *Nat Microbiol*. 2016;2(3):1-6.

46. Martin M. Cutadapt removes adapter sequences from high-throughput sequencing reads. *EMBnet J*. 2011;17(1):10-12.

47. Callahan BJ, McMurdie PJ, Rosen MJ, Han AW, Johnson AJA, Holmes SP. DADA2: High-resolution sample inference from Illumina amplicon data. *Nat Methods*. 2016;13(7):581-583.

48. Ortiz-Burgos S. Shannon-Weaver Diversity Index BT - Encyclopedia of Estuaries. In: Kennish MJ, ed. Springer Netherlands; 2016:572-573. doi:10.1007/978-94-017-8801-4_233

49. McMurdie PJ, Holmes S. Phyloseq: A bioconductor package for handling and analysis of high-throughput phylogenetic sequence data. *Pacific Symp Biocomput*. Published online 2012:235-246. doi:10.1142/9789814366496_0023

50. Harrell Jr FE, Harrell Jr MFE. Package 'hmisc.' *CRAN2018*. 2019;2019:235-236.

51. Bates D, Mächler M, Bolker BM, Walker SC. Fitting linear mixed-effects models using lme4. *J Stat Softw*. 2015;67(1). doi:10.18637/jss.v067.i01

52. Lüdecke D, Ben-Shachar M, Patil I, Waggoner P, Makowski D. performance: An R Package for Assessment, Comparison and Testing of Statistical Models. *J Open Source Softw*. 2021;6(60):3139. doi:10.21105/joss.03139

53. Fiès JC. Analysis of soil textural porosity relative to skeleton particle size, using mercury porosimetry. *Soil Sci Soc Am J*. 1992;56(4):1062-1067.

54. Carminati A, Kaestner A, Ippisch O, et al. Water flow between soil aggregates. *Transp Porous Media*. 2007;68(2):219-236. doi:10.1007/s11242-006-9041-z

55. Kautz T. Research on subsoil biopores and their functions in organically managed soils: A review. *Renew Agric Food Syst*. 2015;30(4):318-327. doi:10.1017/S1742170513000549

56. Ping CL. Gelisols: Part I. Cryogenesis and State Factors of Formation. *Soil Horizons*. 2013;54(3):0. doi:10.2136/sh2013-54-3-gc

57. Withers PJ, Bouman C, Carmignato S, et al. X-ray computed tomography. *Nat Rev Methods Prim*. 2021;1(1). doi:10.1038/s43586-021-00015-4

58. Feng Y, Wang J, Bai Z, Reading L, Jing Z. Three-dimensional quantification of macropore networks of different compacted soils from opencast coal mine area using X-ray computed tomography. *Soil Tillage Res*. 2020;198(29):104567. doi:10.1016/j.still.2019.104567

59. Nimmo JR. *Porosity and Pore Size Distribution*. Published by Elsevier Inc.; 2013. doi:10.1016/b978-0-12-409548-9.05265-9

60. Zhao D, Xu M, Liu G, et al. Quantification of soil aggregate microstructure on abandoned cropland during vegetative succession using synchrotron radiation-based micro-computed

tomography. *Soil Tillage Res*. 2017;165:239-246. doi:10.1016/j.still.2016.08.007

61. Cnudde V, Boone MN. High-resolution X-ray computed tomography in geosciences: A review of the current technology and applications. *Earth-Science Rev*. 2013;123:1-17. doi:10.1016/j.earscirev.2013.04.003

62. Douglas TA, Waldrop MP. Changes in the Active , Dead , and Dormant Microbial Chronosequence. *Appl Environ Microbiol*. 2019;(November 2018):1-16.

63. Blazewicz SJ, Barnard RL, Daly RA, Firestone MK. Evaluating rRNA as an indicator of microbial activity in environmental communities: Limitations and uses. *ISME J*. 2013;7(11):2061-2068. doi:10.1038/ismej.2013.102

64. Saidi-Mehrabad A, Neuberger P, Cavaco M, Froese D, Lanoil B. Optimization of subsampling, decontamination, and DNA extraction of difficult peat and silt permafrost samples. *Sci Rep*. 2020;10(1):1-10. doi:10.1038/s41598-020-71234-0

65. Blagodatskaya E, Kuzyakov Y. Active microorganisms in soil: Critical review of estimation criteria and approaches. *Soil Biol Biochem*. 2013;67:192-211. doi:10.1016/j.soilbio.2013.08.024

66. Bottos EM, Kennedy DW, Romero EB, et al. Dispersal limitation and thermodynamic constraints govern spatial structure of permafrost microbial communities. *FEMS Microbiol Ecol*. 2018;94(8):1-14. doi:10.1093/femsec/fiy110

67. Lydolph MC, Jacobsen J, Arctander P, et al. Beringian paleoecology inferred from permafrost-preserved fungal DNA. *Appl Environ Microbiol*. 2005;71(2):1012-1017. doi:10.1128/AEM.71.2.1012-1017.2005

68. Bellemain E, Davey ML, Kauserud H, et al. Fungal palaeodiversity revealed using high-throughput metabarcoding of ancient DNA from arctic permafrost. *Environ Microbiol*. 2013;15(4):1176-1189. doi:10.1111/1462-2920.12020

69. Sparrman T, Öquist M, Klemedtsson L, Schleucher J, Nilsson M. Quantifying unfrozen water in frozen soil by high-field 2H NMR. *Environ Sci Technol*. 2004;38(20):5420-5425. doi:10.1021/es0493695